Mecánica Computacional Vol. XXIV
A. Larreteguy (Editor)
Buenos Aires, Argentina, Noviembre 2005

CONSIDERATION OF A BIAXIALLY LOADED PHOTOELASTIC PLATE WITH AN ELLIPTICAL DISCONTINUITY USING AN INVERSE PROBLEM METHODOLOGY

Jaime F. Cárdenas-García[*] and Sergio Preidikman[†]

[*] Department of Engineering
The University of Texas at Brownsville
80 Fort Brown, Brownsville, Texas 78520, USA
e-mail: jaime.cardenas@utb.edu

[†] Facultad de Ingeniería
Universidad Nacional de Río Cuarto
Ruta Nacional 36 Km 601, 5800 Río Cuarto, Argentina
e-mail: spreidik@vt.edu

Key words: Inverse Problem Methodology, Finite Element Analysis, Photoelasticity, Elliptical Holes, Optimization, Least Squares Approach.

Abstract. *The direct problem of an elliptical hole in a uniaxially and biaxially loaded, homogeneous, isotropic infinite plate in plane stress is a classical result that has been extensively studied, especially in relation to the assessment of cracks in plates. This theoretical formulation leads naturally into consideration of relevant inverse problems based on using full field stress data, in the form of photoelastic fringes or lines of maximum shear stress. The resulting inverse problems are twofold: (a) from known geometry, biaxial loading and photoelastic response around the elliptical hole determine the material stress fringe value; and, (b) from known geometry, stress fringe value and photoelastic response around the elliptical hole determine the applied far-field loads. Modeling of the elliptical hole in a plate is approached analytically and using finite elements (FE). The inverse problem methodology used relies on least-squares optimization. Initial comparison between the analytical and FE approaches shows that for the experimental results of interest the FE approach should yield better comparisons. Application of the inverse problem methodology allows seamless integration between the FE model results and experimental photoelastic results. The robustness of this approach is tested using noisy data.*

1 INTRODUCTION

The existence of discontinuities in structures is a recurring theme in the research and design literature due to stress concentration concerns that arise due to their presence. The result is that classical theoretical analytical solutions have been developed for circular[1] and elliptical holes[2] in homogeneous, isotropic infinite plates, apart from complete treatises dealing with many other kinds of discontinuities and even considering orthotropic materials[3,4], in an attempt to deal with standard and nonstandard hole shapes. Additionally, much experimental work related to this topic has contributed to a better understanding of the relevant issues by verifying these analytical solutions using photoelasticity[5-9]. Theoretical and experimental work also exists for finite width plates[10,11], and for finite thickness plates[12]. All of these theoretical and experimental approaches may be categorized as direct or forward problem solutions for the discontinuities of interest, i.e., given a material of interest with known material properties, geometry and boundary conditions the objective is to define the stress, strain and/or displacement field over a region of interest. It is also possible, limiting the field of inquiry only to consideration of the stress field, to consider the inverse or reverse problem, i.e., given the geometry and full field stress response, the goal is now to determine the boundary stresses. When posed in this fashion, the infinite plate with a circular hole may be used as a means of separation of stresses and for residual stress determination[5,13-19].

The purpose of this paper is to consider the application and implications of an inverse problem methodology to a biaxially loaded, homogeneous, isotropic plate in plane stress with a centrally located elliptical hole, using full field data in the form of photoelastic fringes or lines of maximum shear stress[20,21]. Two inverse problems are posed: (a) from known geometry, biaxial loading and photoelastic response around the elliptical hole determine the material stress fringe value, i.e., the optical calibration constant of the material; and, (b) from known geometry, stress fringe value and photoelastic response around the elliptical hole determine the applied far-field loads, i.e., the problem of separation of stresses.

2 EXPERIMENTAL RESULTS

In an attempt to deal with these two problems the classical experimental results by Durelli and Murray[6] are analyzed. This experimental work uses a Bakelite (BT-61-893) square plate model approximately 146-mm (5.75-inches) per side, with a central ellipse whose major (2a = 25.4-mm) and minor (2b = 12.7-mm) axes align with the horizontal and vertical edges of the plate, respectively, whose plate thickness is 6.15-mm (0.242-inches). The plate is biaxially loaded by vertical and horizontal far field stresses σ_1 and σ_2, respectively, as shown schematically in Figure 1. Points A and B in Figure 1 refer to the points on the periphery of the elliptical hole that coincide with the *y*- and *x*-axes, respectively. The normal stresses at points A and B, σ_A and σ_B, are directed parallel to the *x*- and *y*-axis, respectively. Table I summarizes the set of experimental results that are presented in their paper, with the gray coloring representing the cases that were analyzed and whose results are included in this paper. The results shown in Table I are obtained from the following equations derived by Durelli and Murray[6] which yield the values at points A and B from known far field stresses,

$$\sigma_A = \sigma_2\left(1+2\frac{b}{a}\right)-\sigma_1 \text{ and } \sigma_B = \sigma_1\left(1+2\frac{a}{b}\right)-\sigma_2 \tag{1}$$

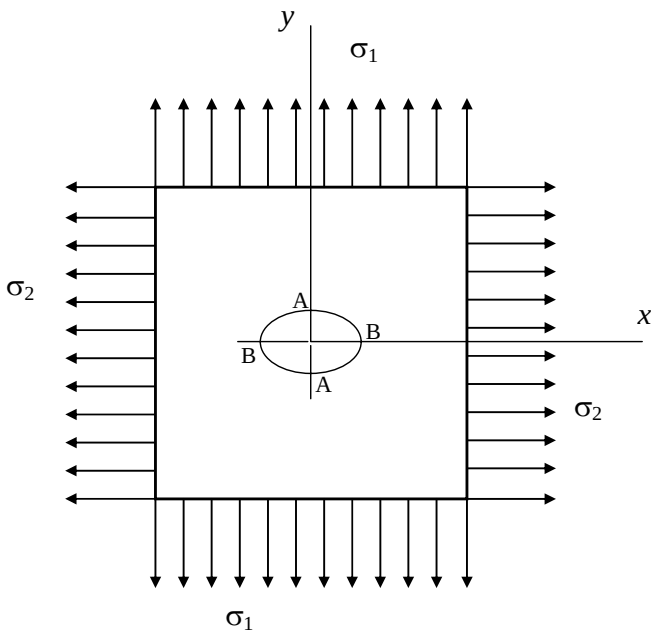

Figure 1: Schematic of a plate with an elliptical hole in biaxial tension in Durelli and Murray [6]

Table 1: Isochromatic Values for Experiments in Durelli and Murray [6]

$k = \sigma_1/\sigma_2$	σ_1	σ_2	σ_A	σ_B
- 3	-2	2/3	3-1/3	- 10-2/3
- 2	-2	1	4	- 11
- 1	-2	2	6	- 12
- 0.56	- 1.25	2.22	5.7	- 8.5
- 1/3	- 1.06	3.22	7.5	- 8.5
- 1/6	- 1/2	3	6.5	- 5.5
0	0	3	6	- 3
0.17	2/3	3.83	7	- 0.5
0.2	0.78	3.89	7	0
0.225	0.89	3.95	7	0.5
0.4	1.17	2.93	4.7	2.9
0.5	1.83	3.67	5.5	5.5
1	3.2	3.2	3.2	12.8
2	2.66	1.33	0	12
4.3	2.62	0.61	- 1.4	12.5
6	2	1/3	- 1.33	9.66
11	2.45	0.22	- 2	12
∞	3.1	0	- 3.1	15.5

It is possible to resolve the inverse problem alluded to above by using these equations, i.e., to obtain the far field stresses σ_1 and σ_2 from knowing the stresses at the periphery of the elliptical hole at points A and B. By algebraic manipulations for a = 2b, the values for σ_1 and

σ_2 are,

$$\sigma_1 = (\sigma_A + 2\sigma_B)/9 \quad \text{and} \quad \sigma_2 = (5\sigma_A + \sigma_B)/9 \tag{2}$$

A review of the stress-optic law, for monochromatic light, is necessary at this point to understand the formation of isochromatic fringes (lines of equal level of extinction or constant maximum shear stress). Maxwell in 1853 noted that the changes in the indices of refraction of a material exhibiting double refraction are linearly proporcional to the loads, and thus related to stresses and strains[20, 21]. For two-dimensional plane-stress bodies, the stress-optic law for light at normal incidence to the plane of a transparent model is written as

$$\Delta = (2\pi t\, c/\lambda)(\sigma_1 - \sigma_2) \tag{3}$$

where Δ is the relative retardation developed between components of a light beam propagating normal to the plane of the plate, t is the plate thickness, c is the speed of light, λ is the wavelength of light, and σ_1 and σ_2 are the in-plane principal stresses. This form is usually further simplified to

$$\sigma_1 - \sigma_2 = n\, f_\sigma / t \tag{4}$$

where $n = \Delta / 2\pi$ is the relative retardation in terms of cycles of retardation, and counted as the fringe order n, and the material fringe value f_σ is a property of the model material for a given wavelength of light, i.e., $f_\sigma = \lambda / c$. Equation (4) may be re-written as

$$\tau_{\max} = (\sigma_1 - \sigma_2)/2 = n\, f_\sigma / 2t \tag{5}$$

which implies that the maximum shear stress [or the prinicpal stress difference $(\sigma_1 - \sigma_2)$] may be determined from measuring the relative retardation or fringe order n, and by ascertaining the value of the material fringe value f_σ by means of calibration. Also, it is clear that the order of extinction n depends on the principal stress difference and the wavelength of the light λ. When the transparent model is viewed in monochromatic light, in a dark-field polariscope arrangement, the isochromatic fringe pattern appears as a series of dark bands since the intensity of the light is zero when n = 0, 1, 2, 3, … For a light filed polariscope arrangement, the intensity of light is zero when n = 0.5, 1.5, 2.3, …

Note that at the hole boundary, e.g., at point A, the maximum shear stress expression is[20]

$$\tau_{\max} = (\sigma_A - 0)/2 = n_A\, f_\sigma / 2t \tag{6}$$

where n_A is the fringe order at point A, f_σ is the material stress fringe value, and t is the plate thickness, following the stress-optic law.

This implies that the stress at point A is given by

$$\sigma_A = f_\sigma n_A / t \tag{7}$$

The same is true for point B, with the implication that equations (2) may be re-written in terms of the fringe orders as follows,

$$\sigma_1 = (f_\sigma / t)(n_A + 2n_B)/9 \quad \text{and} \quad \sigma_2 = (f_\sigma / t)(5n_A + n_B)/9 \tag{8}$$

Table I is a reflection of this practice in Durelli and Murray[6]. This means that no value for

material stress fringe value is specified and it is not possible, given the information in this reference, to resolve the first inverse problem posed above, i.e., from known geometry, biaxial loading and photoelastic response around the elliptical hole to determine the material stress fringe value. Ultimately what this means is that all stress values are given in terms of fringe order values.

3 THEORY: THE ELLIPTICAL HOLE IN A BIAXIALLY LOADED PLATE

In examining the experimental results, the first issue that needs to be dealt with is the issue of whether a theoretical analytical formulation for the biaxially loaded infinite plate is sufficient to describe the experimental results, or whether a finite element (FE) model is needed to better approximate them if the experimental results are more reflective of a finite width plate. To begin and to lend generality to the theoretical approach under consideration the plate material is assumed orthotropic[3,22,23]. Figure 2 shows a schematic of a homogeneous, anisotropic uniaxially loaded infinite plate with an elliptical hole.

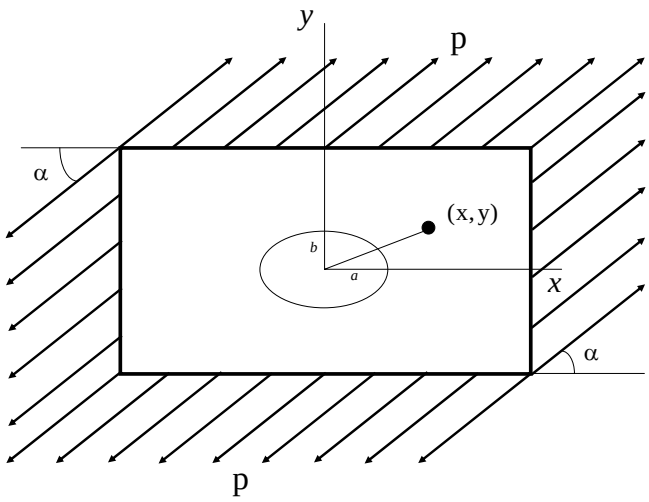

Figure 2: Schematic of a plate with an elliptical hole in uniaxial tension (adapted from Savin [3])

The coordinate axes are chosen in the directions of the principal ellipse axes, where the semi-axes of the ellipse are denoted by *a* and *b*. The load *p* is applied on the plate at an angle α from the horizontal. The equations that describe the normal and shear stresses, respectively, are given by Savin[3] as,

$$\begin{aligned}
\sigma_x(x,y) &= p\cos^2\alpha + 2\,\mathrm{Re}\left[s_1^2\Phi_o'(z_1) + s_2^2\Psi_o'(z_2)\right] \\
\sigma_y(x,y) &= p\sin^2\alpha + 2\,\mathrm{Re}\left[\Phi_o'(z_1) + \Psi_o'(z_2)\right] \\
\tau_{xy}(x,y) &= p\sin\alpha\cos\alpha - 2\,\mathrm{Re}\left[s_1\Phi_o'(z_1) + s_2\Psi_o'(z_2)\right]
\end{aligned} \tag{9}$$

where “Re” in equation (9) means the real part of the complex expression in brackets, where, $s_1 = \alpha_1 + i\,\beta_1$ and $s_2 = \alpha_2 + i\,\beta_2$ are the complex roots of the characteristic equation

$$a_{11}\ s^4 - 2\,a_{16}\,s^3 + (2\,a_{12} + a_{66})\,s^2 - 2\,a_{26}\,s + a_{22} = 0 \tag{10}$$

and the a_{ij}'s are defined in terms of the elastic constants, for the specially orthotropic case, as follows,

$$a_{11} = 1/E_1;\ a_{22} = 1/E_2;\ a_{12} = -\nu_{12}/E_1 = -\nu_{21}/E_2;\ a_{16} = 0;\ a_{26} = 0;\ a_{66} = 1/G_{12} \tag{11}$$

The complex functions $\Phi_o^{'}(z_1)$ and $\Psi_o^{'}(z_2)$ take the form,

$$\Phi_o^{'}(z_1) = \frac{i}{2(s_1 - s_2)}\frac{pb}{a + is_1 b}\left\{1 - \frac{z_1}{\sqrt{z_1^2 - \left(a^2 + s_1^2 b^2\right)}}\right\} \tag{12}$$

$$\Psi_o^{'}(z_2) = \frac{i}{2(s_1 - s_2)}\frac{pb}{a + is_2 b}\left\{1 - \frac{z_2}{\sqrt{z_2^2 - \left(a^2 + s_2^2 b^2\right)}}\right\} \tag{13}$$

for complex quantities $z_1 = x + s_1$ y and $z_2 = x + s_2\,y$. Given this theoretical formulation that is applicable to orthotropic materials it is possible to derive the equations for the isotropic case by setting $s_1 = 1.001 \cdot i$ and $s_2 = 0.999 \cdot i$. This then defines the stress state $\left(\sigma_x,\ \sigma_y,\ \tau_{xy}\right)_i$ at any point $\left(x_i,\ y_i\right)$ around the elliptical hole for any applied uniaxial stress. To obtain the needed biaxial stress state, as required for the experimental results by Durelli and Murray[6], the principle of superposition is applied for the case where $\alpha = \pi/2$ and $p = \sigma_1$, and the case where $\alpha = 0$ and $p = \sigma_2$, schematically shown in Figure 1. The composite equations that are obtained are the solution to the direct problem, from which the isochromatic fringes, or lines of maximum shear stress are used to represent the full field stresses. The stress-optic law is expressed by the equation[20, 21],

$$\tau_{\max} = (p - q)/2 = n\ f_\sigma/2t = \left[\left(\left(\sigma_x - \sigma_y\right)/2\right)^2 + \tau_{xy}^2\right]^2 \tag{14}$$

where p and q are the principal stresses at a point, n is the fringe order, f_σ is the material stress fringe value, and t is the plate thickness. Based on these equations the stress field and resulting isochromatics or lines of maximum shear surrounding an elliptical hole in an isotropic biaxially loaded infinite plate are generated for any set of far field stresses σ_1 and σ_2. Recall that all maximum shear stress and other stress values may be specified as fringe orders.

4 THEORY: THE FINITE ELEMENT MODEL FOR A FINITE PLATE

Figure 3 shows the discretized model used in implementing the finite element model.

Symmetry considerations allow only a quarter of the plate to be used. The plate size is comparable to that of the experiment, i.e., for the quarter plate model each side is approximately 73-mm (2.875-inches) per side, with a central ellipse whose major (a = 12.7-mm) and minor (b = 12.7-mm) semi-axes align with the horizontal and vertical edges of the plate, respectively, for plate thickness of 6.15-mm (0.242-inches). The model uses three-node triangular isoparametric plane-stress elements, and includes 16,096 elements and 64,930 nodes. The left and lower boundaries of the model have been constrained to not move in the x- and y-directions, respectively. The upper and right boundaries are subjected to the applied normal stresses, σ_1 and σ_2, respectively.

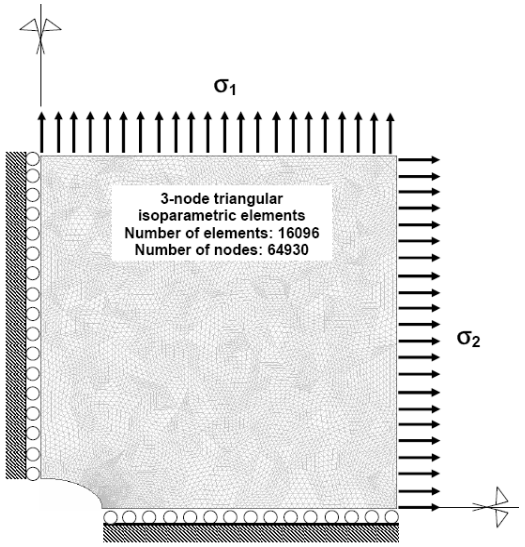

Figure 3: Schematic diagram of the finite element mesh and boundary conditions of the symmetric quarter-plate with an elliptical hole in biaxial tension

5 THE INVERSE PROBLEM METHODOLOGY

The *direct* or *forward* analytical and FE solutions presented in the previous sections are the basis to implement an *inverse* or *reverse* problem methodology to resolve the problem of separation of stresses. Figure 4 shows the inverse problem methodology that is applied in the solution of the analytical problem, and is easily adapted for use with the FE solution. The implementation procedure evolves from the initial *direct* problem definition that defines the full field stresses in the infinite plate with an elliptical hole. Following the outer path of the block diagram the input parameters: plate geometry, elliptical hole size, material properties, boundary conditions (loads and constraints); and, output parameters: full field stresses and isochromatics, are defined. Once these assumptions are made and the model is implemented it is possible to generate the output values at any number of points in the model, generating data files that include the isochromatic fringe order at a corresponding Cartesian coordinate location. These simulated data sets are analogous to actual experimental data which are saved in a file as if it was data collected from an actual experiment. Figure 5 shows a plot of the isochromatic lines, or lines of maximum shear stress[20, 21], for the analytical solution for an

infinite plate with an elliptical hole given the geometric properties defined above, for far field stress loads of $\sigma_1 = 13.80\,MPa$ and $\sigma_2 = 6.90\,MPa$, and a material stress fringe value of $f_\sigma = 15.87\,kPa - m/\,fringe$.

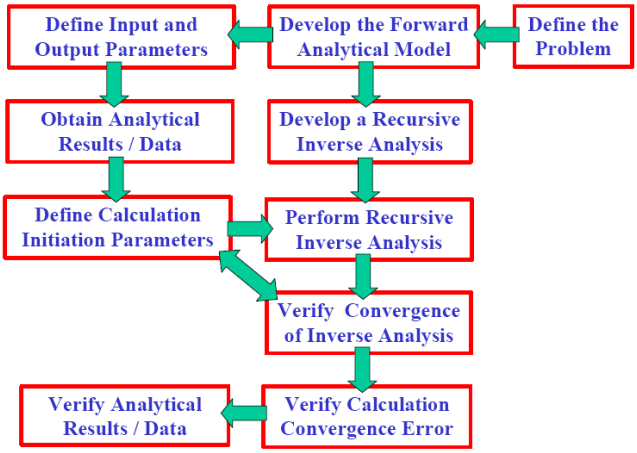

Figure 4: The Inverse Problem Methodology

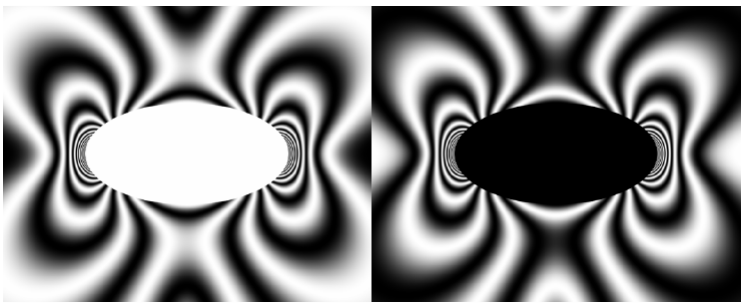

Figure 5: Analytically Calculated Full Field Isochromatics for the Infinite Plate with an Elliptical Hole (a/b =2) ;far field loads: $\sigma_1 = 13.80\,MPa$ and $\sigma_2 = 6.90\,MPa$, $f_\sigma = 15.87\,kPa - fringe/m$, $t = 6.15\ mm$

5.1 Comparison of the Analytical and Finite Element Models

The results shown in Figure 5 may be compared qualitatively to those shown in Figure 6 taken from Durelli and Murray[6]. Notice that Figure 6 shows asymmetrical features which are clearly not evident in Figure 5. At this point only a qualitative comparison is possible since no systematic approach to making a quantitative comparison has been presented. A question that arises from a cursory comparison of Figures 5 and 6 is whether or not the theoretical representation shown in Figure 5 may be used to accurately represent an experimental result such as that of Figure 6. One approach to verifying this is to compare the analytical representation to a finite element (FE) simulation. Figure 7 shows a sequence of images calculated using the previously described FE model: (a) one, (b) two, (c) four, and (d) 16 times the experimental plate size. Careful scrutiny of these images shows significant variation between (a) and (d), but not between (c) and (d). Also, when images 7(d) are compared to the

images in Figure 5 they are clearly the same. In summary, when a comparison is made between the analytical and the FE models, there is clear coincidence between these two models for a FE model plate size of 16 times the experimental model. In conclusion, the FE model is more relevant if what is needed is to compare these FE model results to the experimental results in Durelli and Murray[6]. Therefore, the FE model will be used to implement the inverse problem methodology described in this paper, rather than the analytical solution.

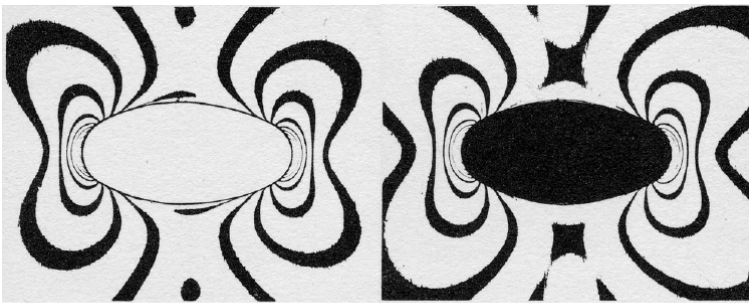

(a) Light field (b) Dark field

Figure 6: Experimental Full Field Isochromatics for the Infinite Plate with an Elliptical Hole (a/b = 2); far field loads: $\sigma_1 = 2.66$ and $\sigma_2 = 1.33$; $\sigma_A = 0$ and $\sigma_B = 12$, $t = 6.15\ mm$ (adapted from [6])

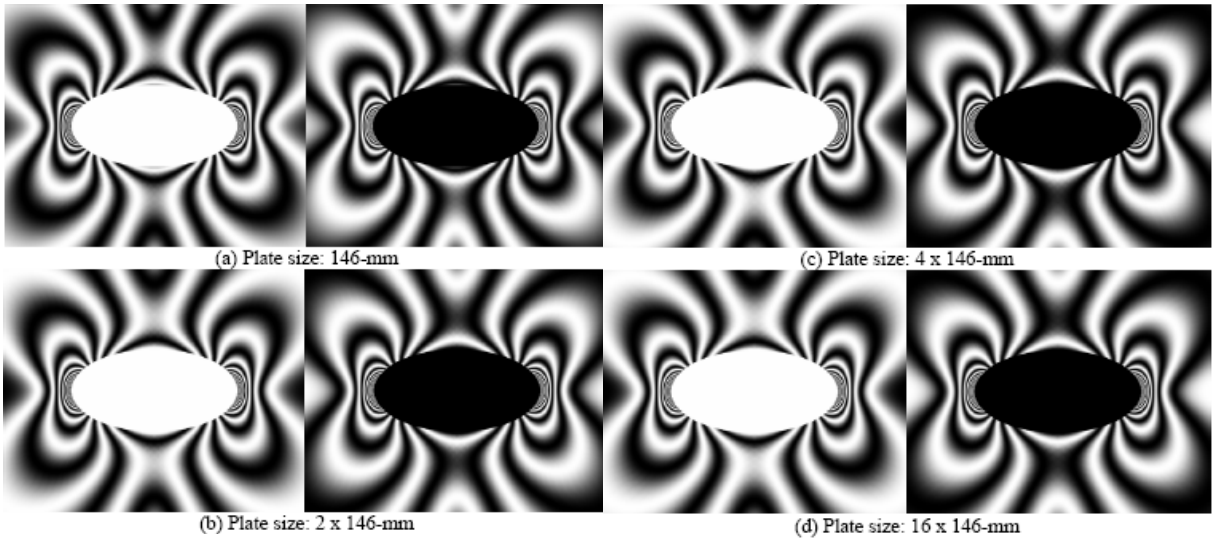

Figure 7: Finite Element Calculated Full Field Isochromatics for the Finite Plate with an Elliptical Hole (a/b = 2); far field loads: $\sigma_1 = 13.80\,MPa$ and $\sigma_2 = 6.90\,MPa$, $f_\sigma = 15.87\,kPa - fringe/m$, $t = 6.15\ mm$

5.2 Optimization Approach

Referring back to Figure 4, but now following the inner path, a recursive inverse problem procedure needs implementation using the previously generated simulated experimental data sets. In implementing these recursive inverse problem procedures, initial values for the

parameters of interest, i.e., the boundary stresses σ_1 and σ_2 need to be defined and re-defined, if appropriate, to verify convergence. Once convergence is verified an assessment is made as to the success in generating the analytical input values used to solve the direct problem initially solved. The recursive inverse problem procedure that is implemented relies on nonlinear least squares, which in its simplest form follows a Newton-Raphson approach[21, 24-27], as described below, and can easily be adapted to a Levenberg-Marquardt approach[28, 29]. Briefly, to implement this inverse problem for stress isochromatics the objective function that describes the relationship between experimental and FE calculated results is

$$\left[F_i(\sigma_1,\sigma_2)\right]_{\text{Experimental}} = \left[F_i(\sigma_1,\sigma_2)\right]_{\text{FE}} + e_i \tag{15}$$

where, $\left[F_i(\sigma_1,\sigma_2)\right]_{\text{Experimental}}$ represents the experimental fringe order data at some point (x_i, y_i) in the specimen; $\left[F_i(\sigma_1,\sigma_2)\right]_{\text{FE}}$ represents the FE evaluation at the same point, with undetermined coefficients (σ_1,σ_2), the applied specimen boundary stresses; and, e_i is the random error. This equation implies that the random error is zero if the FE program exactly predicts the experimental values at every point on the specimen. The goal in this exercise is to minimize the errors in the objective function. More specifically, the experimental values are represented by the fringe order data at each point in the specimen, i.e.,

$$\left[\left(\tau_{\max}\right)_i\right]_{\text{Experimental}} = \left[\left(\sigma_1\right)_i - \left(\sigma_2\right)_i\right]/2 = n_i f_\sigma / 2t \tag{16}$$

As mentioned previously, only fringe orders are used to make assessment of stresses in the experimental model. The numerical values for the stress state at each corresponding point on the specimen from the FE model are given by $\left(\sigma_x\right)_i$, $\left(\sigma_y\right)_i$, and $\left(\tau_{xy}\right)_i$, from which values for maximum shear stress, $\left[\left(\tau_{\max}\right)_i\right]_{\text{FE}}$, are obtained, all in fringe orders units. The maximum shear stress values obtained from the FE model are,

$$\left[\left(\tau_{\max}\right)_i\right]_{\text{Numerical}} = \sqrt{\left[\left(\left(\sigma_x\right)_i - \left(\sigma_y\right)_i\right)/2\right]^2 + \left[\left(\tau_{xy}\right)_i\right]^2} \tag{17}$$

This results in the following functional after rearranging Equation (15),

$$F_i(\sigma_X,\sigma_Y,\tau_{XY}) = \left[\left(\tau_{\max}\right)_i\right]^2_{\text{Numerical}} - \left[\left(\tau_{\max}\right)_i\right]^2_{\text{Experimental}} = 0 \tag{18}$$

or,

$$F_i(\sigma_X,\sigma_Y,\tau_{XY}) = \left\{\left[\left(\sigma_x\right)_i - \left(\sigma_y\right)_i/2\right]^2 + \left[\left(\tau_{xy}\right)_i\right]^2\right\} - \left\{n_i f_\sigma / t\right\}^2 = 0 \tag{19}$$

A Taylor's series expansion of Equation (19) leads to,

$$\left(F_i\right)_{k+1} = \left(F_i\right)_k + \left(\partial F_i/\partial\sigma_1\right)_k \Delta\sigma_1 + \left(\partial F_i/\partial\sigma_2\right)_k \Delta\sigma_2 + H.O.T. \tag{20}$$

where *k* refers to the *kth* iteration step, $\Delta\sigma_1$ and $\Delta\sigma_2$ are corrections to the previous estimates of σ_1 and σ_2, respectively, and $H.O.T.$ stands for Higher Order Terms. The explicit relations for the correction terms are,

$$\Delta\sigma_1 = (\sigma_1)_{k+1} - (\sigma_1)_k \; ; \quad \Delta\sigma_2 = (\sigma_2)_{k+1} - (\sigma_2)_k \tag{21}$$

For experimental and FE calculated values that are close to each other implies that $(F_i)_{k+1}$ in Equation (20) approaches zero. Reordering Equation (20) and expressing it in matrix form, for *m* data points,

$$\{F\} = [a]\{\Delta\sigma\} \tag{22}$$

where

$$\{F\}_k = \begin{Bmatrix} -F_1 \\ -F_2 \\ \vdots \\ -F_m \end{Bmatrix}_k \; ; \quad [a]_k = \begin{bmatrix} \dfrac{\partial F_1}{\partial \sigma_1} & \dfrac{\partial F_1}{\partial \sigma_2} \\ \dfrac{\partial F_2}{\partial \sigma_1} & \dfrac{\partial F_2}{\partial \sigma_2} \\ \vdots & \vdots \\ \dfrac{\partial F_m}{\partial \sigma_1} & \dfrac{\partial F_m}{\partial \sigma_2} \end{bmatrix}_k \; ; \quad \{\Delta\sigma\} = \begin{Bmatrix} \Delta\sigma_1 \\ \Delta\sigma_2 \end{Bmatrix} \tag{23}$$

Pre-multiplication of Equation (22) by $[a]^T$, and solving for the correction factors $\{\Delta\sigma\}$ yields, $\{\Delta\sigma\} = [c]^{-1}[a]^T\{F\}$, where $[c] = [a]^T[a]$. This iteration process ends when an acceptable pre-defined convergence value is attained.

5.3 Examples: Finite Element Based Calculation of Boundary Stresses

The procedures outlined in Figure 4 and explained above are implemented and tested using computer generated data to obtain the far field stresses for the analytical model. This is equivalent to solving the problem of separation of stresses. One way to assess the validity of this inverse problem methodology is to examine its robustness by adding noise to the full field isochromatics data and to test for: (a) the ability to recover the original far field stresses; and, (b) whether all regions around the periphery of the hole have the same influence in recovering the far field stresses. Similar conclusions should apply to FE based results.

Random error in the stress isochromatics - The addition of noise to computer generated experimental data is equivalent to experimental measurements which oftentimes includes noise or random error. Noisy data allows determining how much noise the nonlinear least squares approach can tolerate. The data files or output files from data collection around the elliptical hole in the plate have added random signals in the calculated maximum shear stress

values. These output files are the input data to implement the inverse problem procedures. The total maximum shear stress, in fringe order units, at every point of interest is modified as follows,

$$\left[\left(\tau_{\max}\right)_{tot}\right]_i = \left(\tau_{\max}\right)_i + \xi \cdot f_\sigma / 2t \cdot RNV_i \tag{24}$$

where the product $\left(\xi f_\sigma / 2t\right)^2$ is the noise variance, and is defined for $0 \le \xi \le 1$ and ratio of fringe value to plate thickness, $f_\sigma / t = 1$ *Pa per fringe*. The intent of arbitrarily setting this ratio to 1 is to work in terms of fringe orders. RNV_i is a normally distributed Random Number Vector, *m* random numbers long, with a mean value of zero, variance $\sigma^2 = 1$, and standard deviation $\sigma = 1$. Two extreme cases of far field stress loading are examined: Case 1 considers $\sigma_1 = 5$ and $\sigma_2 = 0$, or $k = \infty$; and, Case 2 looks at $\sigma_1 = 0$ and $\sigma_2 = 5$, or $k = 0$. Note that $k = \sigma_1 / \sigma_2$ is the ratio of the vertical to the horizontal far-field or applied boundary stresses. Case 2 is shown in Figure 8 for different levels of noise. Even for noise levels of $\xi = 0.70$ and using only 121 points within the noisy stress field of the first quadrant of the plate it was not possible to generate absolute errors greater than 5% in estimating far field stress values of σ_1 and σ_2. Thus, the ability to recover the original far field stresses could be checked; but it was not possible to test whether all regions around the periphery of the hole have the same influence in recovering the far field stresses.

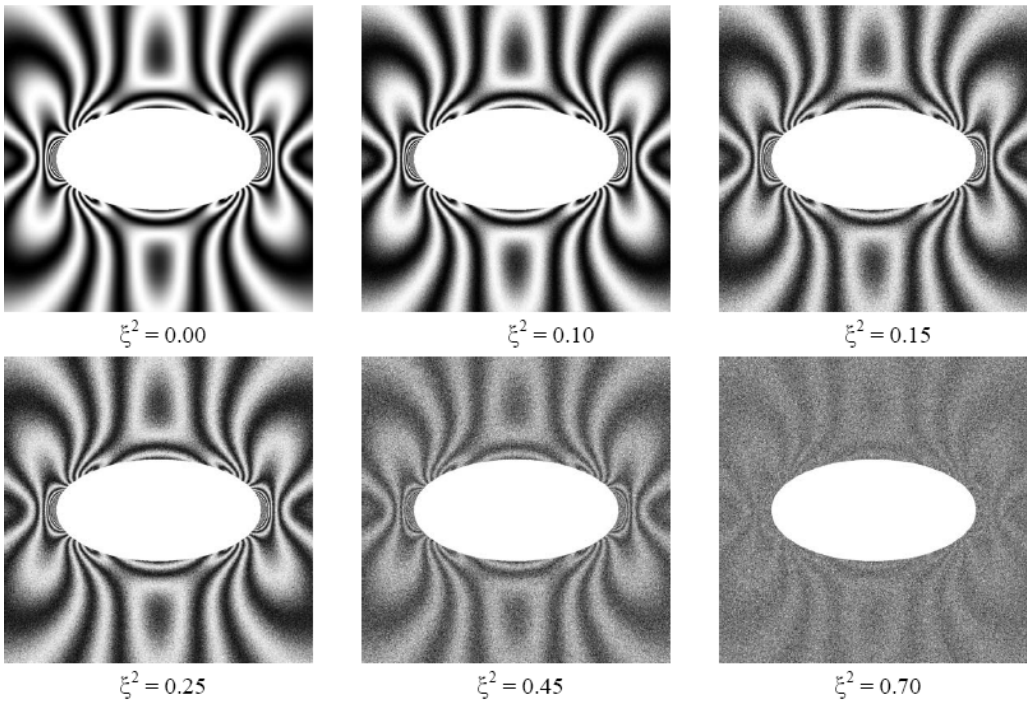

Figure 8: The effect of noise variance, ξ^2, on the light-field isochromatics for $\sigma_1 = 0$, $\sigma_2 = 5$

Finite Element Based Inverse Analysis - Some observations to implement the FE based optimization approach using least squares are needed. To start calculations using the quantities shown in Equation (23), the terms related to $\{F\}_k$ and $[a]_k$ should be defined. Once the starting values of $(\sigma_1)_0$ and $(\sigma_2)_0$, the farfield stresses, are known, the definition of the $\{F\}_k$ values is straightforward. To obtain the partial derivatives $\partial F_1/\partial\sigma_1, \partial F_2/\partial\sigma_1, \ldots, \partial F_m/\partial\sigma_1$, etc., at the initial far field stress values of $(\sigma_1)_0$ and $(\sigma_2)_0$ each partial derivative is treated as follows,

$$\begin{aligned} &\frac{\partial F_1}{\partial \sigma_1} = \frac{\Delta F_1}{\Delta \sigma_1} = \frac{(F_1)_{k-1} - (F_1)_k}{(\sigma_1)_{k-1} - (\sigma_1)_k}, \quad \frac{\partial F_2}{\partial \sigma_1} = \frac{\Delta F_2}{\Delta \sigma_1} = \frac{(F_2)_{k-1} - (F_2)_k}{(\sigma_1)_{k-1} - (\sigma_1)_k}, \\ &\qquad\qquad \vdots \\ &\frac{\partial F_m}{\partial \sigma_1} = \frac{\Delta F_m}{\Delta \sigma_1} = \frac{(F_m)_{k-1} - (F_m)_k}{(\sigma_1)_{k-1} - (\sigma_1)_k}, \quad \frac{\partial F_1}{\partial \sigma_2} = \frac{\Delta F_1}{\Delta \sigma_2} = \frac{(F_1)_{k-1} - (F_1)_k}{(\sigma_2)_{k-1} - (\sigma_2)_k}, \text{ etc.} \end{aligned} \tag{25}$$

This implies that two different sets of starting values for *k = 1*, i.e., $\left[(\sigma_1)_0, (\sigma_1)_1\right]$ and $\left[(\sigma_2)_0, (\sigma_2)_1\right]$ need to be defined. For example, to calculate the *m* values of $\partial F_m/\partial\sigma_1$, values for $(\sigma_1)_0$ and $(\sigma_1)_1$ are assumed. All values of $\{F_m\}_0$ and $\{F_m\}_1$ are calculated, assuming that $(\sigma_2) = (\sigma_2)_0$. In a similar way, to calculate the *m* values of $\partial F_m/\partial\sigma_2$, values for $(\sigma_2)_0$ and $(\sigma_2)_1$ are assumed. All values of $\{F_m\}_0$ and $\{F_m\}_1$ are calculated, assuming that $(\sigma_1) = (\sigma_1)_0$. Once all of the partial derivatives are defined, this allows fully defining $[a]_k$, after which all calculations are performed. This calculation scheme was tested with computer generated data and was found to give excellent results. The intent is now to show the application of the previously defined inverse problem methodology to experimental results in Durelli and Murray[6]. The experimental results used to assess the capabilities in the implementation of the inverse problem methodology are for values of nominal far field stress ratio *k = 0, 1,* and *infinity*. Figure 9 shows a flowchart with the procedures needed to implement the specified calculations. The actual implementation of the activities shown in this chart implies that the recursive inverse analysis procedure is fully tested and is ready to be applied to experimentally generated data. This flowchart shows that a prerequisite is a well-defined forward experimental model, i.e., the design of the biaxial loading of a thin plate in plane stress with a central elliptical hole. The experimental results in Durelli and Murray[6] have fully defined input and output parameters that yield the light and dark full field isochromatics. This allows the harvesting of experimental results/data, which take the form of position coordinates, (x_i, y_i), and corresponding fringe orders, n_i, around the hole in the photoelastic plate. These data sets are then used to perform the recursive inverse analysis. The inverse problem methodology calculations start with the reading of the experimental data values that

are collected. Then, the initiation parameters are established and the needed recursive analysis is performed with an initial attempt to verify convergence. Once convergence is achieved, by modifying the initiation parameters, the calculation convergence error is evaluated. If the initiation parameters are found to be adequate, the results are then verified.

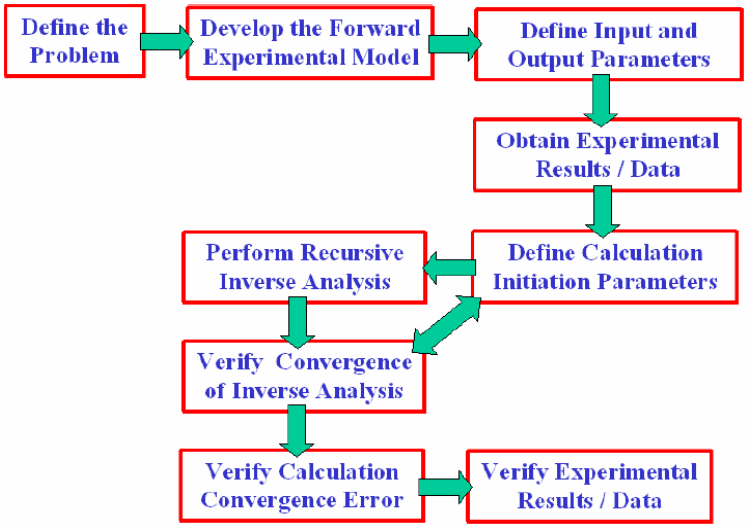

Figure 9: Flowchart Outlining the Experimental Side of the Inverse Problem Methodology

The three previously mentioned experimental results are now examined in detail:

Example 1: This is the first of three examples that analyze experimental results found in Durelli and Murray[6] to assess separation of stresses. Figure 10 shows the light and dark field images chosen for analysis for experimental far field stress values: $\sigma_1 = -2$ and $\sigma_2 = 2/3$, or $k = \sigma_1/\sigma_2 = -3$. These and all images used for analysis are obtained by scanning them at a resolution level of 800 dots per inch from a copy of the journal. Both the light field and dark field isochromatics are analyzed. Data is collected, using SigmaScan/Image™ software, from all four quadrants of the image assuming that the x- and y-axes are located at the center of the elliptical hole.

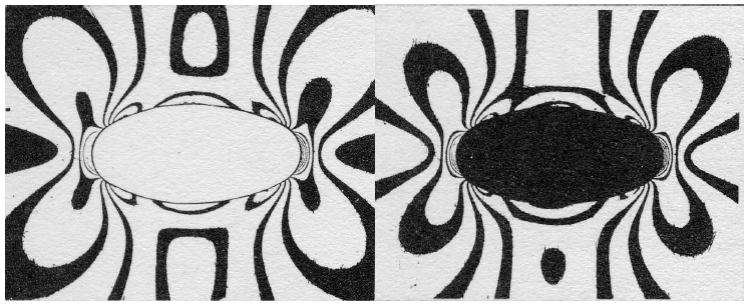

(a) Light field (b) Dark field

Figure 10: Experimental Full Field Isochromatics for the Plate with an Elliptical Hole (a/b = 2); Nominal Far Field Stresses: $\sigma_1 = -2$ and $\sigma_2 = 2/3$; $\sigma_A = 3.333$ and $\sigma_B = -10.667$ (adapted from [6])

Table 2 shows the distribution of the various collected data sets, estimated along the fringe centers, among associated fringe orders and image quadrants. After data collection it was necessary to scale the pixel locations by using the average of the measurement of the major and minor axes of the radius of the hole of 18.60 and 18.86 pixels per millimeter, for the light and dark fields, respectively. Additionally, since the FEM model only considers the top right quadrant of the plate because of symmetry considerations, the collected data sets were folded over to reflect this. This has the potential to add additional error, if the experimental image is not fully symmetric as close examination of the experimental results reveals. An additional source of error is due to rotational misalignment of the experimental image with respect to the axes of symmetry.

Table 2: Fringe Order Data Collection by Quadrant from Experimental Full Field Isochromatics for the Plate with an Elliptical Hole ($a/b = 2$); far field loads: $\sigma_1 = -2$, $\sigma_2 = 2/3$; $\sigma_A = 3.333$, $\sigma_B = -10.667$

Figure	Fringe Order	Number of Data Points				
		Q1	Q2	Q3	Q4	Total
10(a)	1.5	52	40	51	50	193
10(b)	2	68	75	63	55	261
10(a)	2.5	51	53	58	55	217
10(b)	3	66	69	58	52	245
10(a)	3.5	78	92	77	69	316
10(b)	4	55	51	39	47	192
10(a)	4.5	25	18	16	20	79
10(b)	5	15	14	11	15	55
10(a)	5.5	18	15	16	17	66
10(b)	6	10	11	9	10	40
10(a)	6.5	16	0	0	11	27
10(b)	7	9	7	8	11	35

Analysis of the data leads to the values for σ_1 , σ_2 and $k = \sigma_1/\sigma_2$, shown in Table 3a, which shows three sets of results for data sets from the four quadrants and an additional combined data set of all four quadrants: (a) the results on the left correspond to the dark field isochromatics data; (b) the results in the center correspond to the light field isochromatics data; and, (c) the results on the right correspond to the consideration of the combined data sets of light and dark field isochromatics.

Table 3a: Determination of Far Field Stresses using Data from Individual and Combined Quadrants for the Plate with an Elliptical Hole ($a/b = 2$); Far Field Stresses: $\sigma_1 = -2$, $\sigma_2 = 2/3$

	Dark Field Isochromatics			Light Field Isochromatics			Combined Dark and Light Field Isochromatics		
Quadrant	σ_1	σ_2	$k = \sigma_1/\sigma_2$	σ_1	σ_2	$k = \sigma_1/\sigma_2$	σ_1	σ_2	$k = \sigma_1/\sigma_2$
1	-2.31	0.37	-6.26	-2.38	0.32	-7.50	-2.35	0.34	-6.89
2	-2.38	0.34	-6.95	-2.31	0.40	-5.77	-2.35	0.37	-6.36
3	-2.27	0.32	-7.15	-2.21	0.35	-6.35	-2.24	0.33	-6.80
4	-2.37	0.21	-11.07	-2.34	0.27	-8.67	-2.36	0.25	-9.54
1-2-3-4	-2.33	0.32	-7.33	-2.32	0.32	-7.17	-2.33	0.32	-7.25
Reference	-2.00	2/3	-3.00						

In Table 3a the reference values cited by Durelli and Murray[6] are also included. Notice that there is a discrepancy between the calculated values and the reference values: the discrepancy is smaller for the σ_1 value than for the σ_2 value. The calculated values do maintain certain predictability between corresponding data sets. Figures 11 and 12 show the reconstructed composite images using these various data sets and their comparison to the experimental results, for light and dark filed isochromatics, respectively.

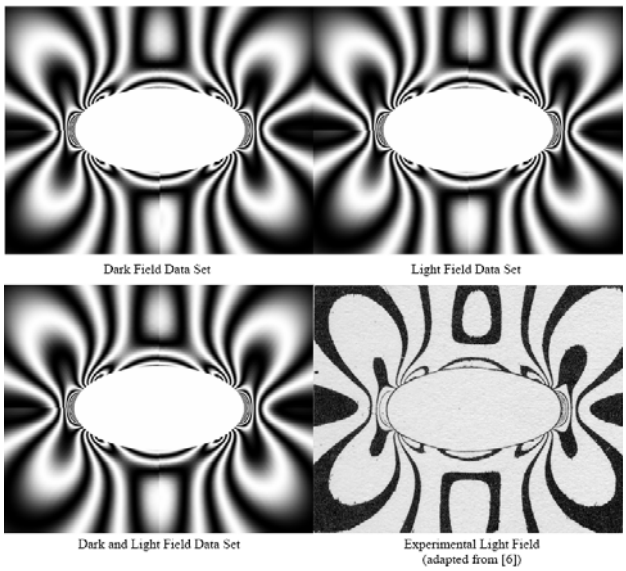

Figure 11: Comparison of Reconstructed and Experimental Light Field Isochromatics for the Plate with an Elliptical Hole (a/b = 2); Nominal Far Field Stresses: $\sigma_1 = -2$ and $\sigma_2 = 2/3$

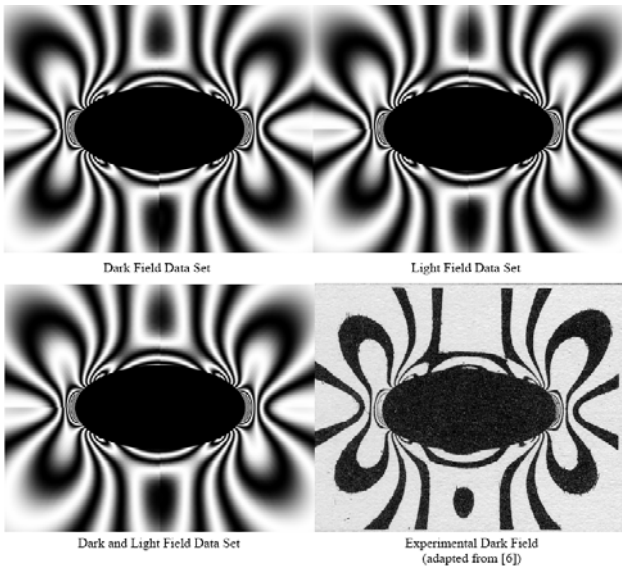

Figure 12: Comparison of Reconstructed and Experimental Dark Field Isochromatics for the Plate with an Elliptical Hole (a/b = 2); Nominal Far Field Stresses: $\sigma_1 = -2$ and $\sigma_2 = 2/3$

Notice that each reconstructed quadrant yields a different stress distribution, which serves to point out the differences that exist between quadrants in the experimental results. These differences also serve to point out that experimental biaxial loading is not perfect, showing the experimental difficulties inherent to implementing biaxial loading. The experimental researchers seem to have greater control when imposing the vertical load, σ_1. Table 3b shows similar results for points A and B identified in Figure 1 for the same parallel values of σ_1 and σ_2 in Table 3a. Similar observations as before may be made, noting that the value for σ_A is closer to its reference value than the value for σ_B. Note that the reference values are applicable to those of an infinite plate.

Table 3b: Determination of Hole Surface Stresses Perpendicular to the *x*-and *y*-axes using Data from Individual and Combined Quadrants for the Plate with an Elliptical Hole ($a/b = 2$); Far Field Stresses: $\sigma_1 = -2$, $\sigma_2 = 2/3$

	Dark Field Isochromatics			Light Field Isochromatics			Combined Dark and Light Field Isochromatics		
Quadrant	σ_A	σ_B	$k_{AB} = \sigma_A/\sigma_B$	σ_A	σ_B	$k_{AB} = \sigma_A/\sigma_B$	σ_A	σ_B	$k_{AB} = \sigma_A/\sigma_B$
1	2.19	12.38	0.18	2.44	12.98	0.19	2.36	12.70	0.19
2	2.29	13.34	0.17	2.26	11.74	0.19	2.23	12.55	0.18
3	2.88	14.68	0.20	2.23	11.61	0.19	2.35	13.05	0.18
4	2.70	13.98	0.19	2.31	12.58	0.18	2.46	13.21	0.19
1-2-3-4	2.47	13.55	0.18	2.30	12.30	0.19	2.34	12.86	0.18
Reference	3.20	12.80	0.25						

Example 2: Tables 4a and 4b, and Figures 13 and 14 show the results for nominal far field stress values of $\sigma_1 = 0$ and $\sigma_2 = 3$, or $k = \sigma_1/\sigma_2 = 0$. The most noticeable feature in the reconstruction of the experimental fringes is that a great discrepancy exists between the left and right hand sides of the images, which reflect what also occurs with the experimental images. This seems to point to some inherent feature of the experimental setup that in some way hinders the application of horizontal or σ_2 far field loads, corroborating the observation made previously for Example 1. Note that the values for σ_1 are approximately zero, and the values of σ_2 are closer to 2.5 than to 3.0. Also, the value for k_{AB} seems to vary widely, reflecting the inconsistency between the left and right sides of the plate.

Table 4a: Determination of Far Field Stresses using Data from Individual and Combined Quadrants for the Plate with an Elliptical Hole ($a/b = 2$); Far Field Stresses: $\sigma_1 = 0$, $\sigma_2 = 3$

	Dark Field Isochromatics			Light Field Isochromatics			Combined Dark and Light Field Isochromatics		
Quadrant	σ_1	σ_2	$k = \sigma_1/\sigma_2$	σ_1	σ_2	$k = \sigma_1/\sigma_2$	σ_1	σ_2	$k = \sigma_1/\sigma_2$
1	0.07	2.50	0.03	0.02	2.49	0.01	-0.02	2.50	-0.01
2	-0.02	2.66	-0.01	0.13	2.67	0.05	0.04	2.66	0.02
3	-0.06	2.64	-0.02	0.03	2.65	0.01	-0.02	2.65	-0.01
4	0.01	2.56	0.00	0.18	2.60	0.07	0.09	2.58	0.03
1-2-3-4	-0.03	2.59	-0.01	0.08	2.60	0.03	0.02	2.60	0.01
Reference	0.00	3.00	0.00						

Table 4b: Determination of Hole Surface Stresses Perpendicular to the *x*- and *y*-axes using Data from Individual and Combined Quadrants for the Plate with an Elliptical Hole ($a/b = 2$); Far Field Stresses: $\sigma_1 = 0$, $\sigma_2 = 3$

	Dark Field Isochromatics			Light Field Isochromatics			Combined Dark and Light Field Isochromatics		
Quadrant	σ_A	σ_B	$k_{AB} = \sigma_A/\sigma_B$	σ_A	σ_B	$k_{AB} = \sigma_A/\sigma_B$	σ_A	σ_B	$k_{AB} = \sigma_A/\sigma_B$
1	5.07	2.42	2.10	5.10	2.67	1.91	5.17	2.90	1.78
2	5.50	3.07	1.79	5.35	2.29	2.34	5.43	2.76	1.97
3	5.50	3.26	1.68	5.42	2.80	1.94	5.48	3.06	1.79
4	5.26	2.80	1.88	5.15	1.94	2.65	5.21	2.40	2.17
1-2-3-4	5.36	3.05	1.76	5.26	2.48	2.13	5.33	2.79	1.91
Reference	6.00	3.00	2.00						

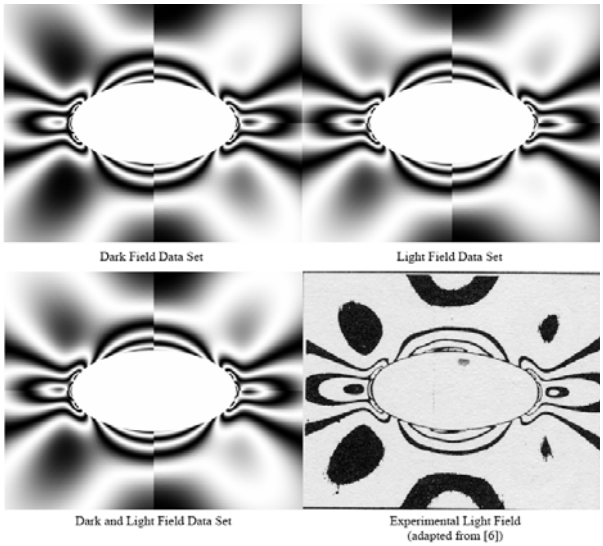

Figure 13: Comparison of Reconstructed and Experimental Light Field Isochromatics for the Plate with an Elliptical Hole (a/b = 2); Nominal Far Field Stresses: $\sigma_1 = 0$ and $\sigma_2 = 3$

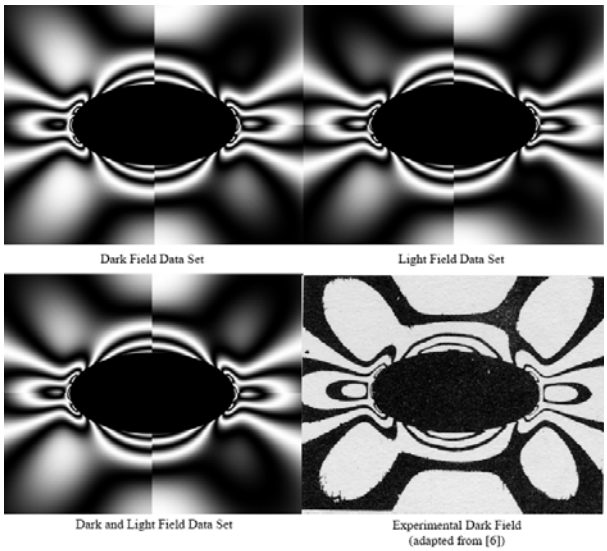

Figure 14: Comparison of Reconstructed and Experimental Dark Field Isochromatics for the Plate with an Elliptical Hole (a/b = 2); Nominal Far Field Stresses: $\sigma_1 = 0$ and $\sigma_2 = 3$

Example 3: Figures 15 and 16, and Tables 5a and 5b show the results for nominal far field stress values of $\sigma_1 = 3.10$ and $\sigma_2 = 0$, or $k = \sigma_1/\sigma_2 = \infty$.

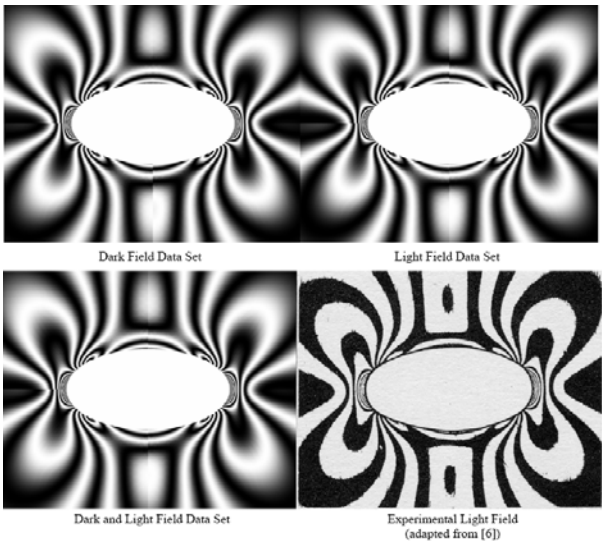

Figure 15: Comparison of Reconstructed and Experimental Light Field Isochromatics for the Plate with an Elliptical Hole (a/b = 2); Nominal Far Field Stresses: $\sigma_1 = 3.1$ and $\sigma_2 = 0$

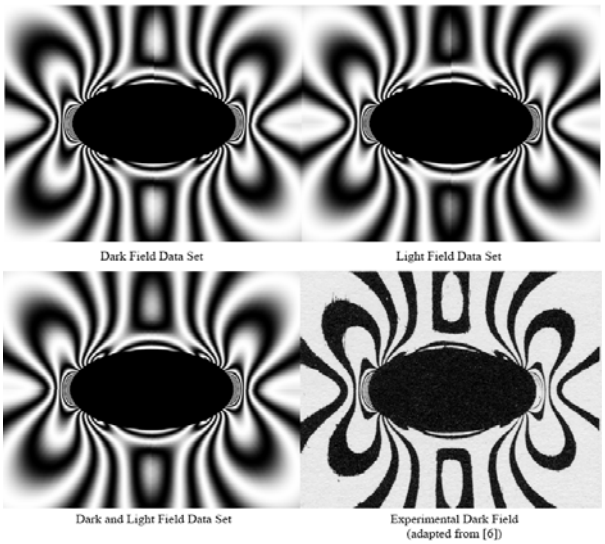

Figure 16: Comparison of Reconstructed and Experimental Dark Field Isochromatics for the Plate with an Elliptical Hole (a/b = 2); Nominal Far Field Stresses: $\sigma_1 = 3.1$ and $\sigma_2 = 0$

The most salient feature in the comparison of Figures 15 and 16 is that though some asymmetry exists between the left side and right side of the experimental result, which is reflected in the reconstructions of the quadrant data; there is less of an asymmetry between the top and bottom portions of the experimental specimen. Note also that the values for σ_2

are approximately zero, and the values of σ_1 are closer to 2.5 than to 3.10. Table 5b also shows that k_{AB} is consistently close to a value of 0.20 which is the theoretical value for the infinite plate.

Table 5a: Determination of Far Field Stresses using Data from Individual and Combined Quadrants for the Plate with an Elliptical Hole ($a/b = 2$); Far Field Stresses: $\sigma_1 = 3.1$, $\sigma_2 = 0$

	Dark Field Isochromatics			Light Field Isochromatics			Combined Dark and Light Field Isochromatics		
Quadrant	σ_1	σ_2	$k = \sigma_1/\sigma_2$	σ_1	σ_2	$k = \sigma_1/\sigma_2$	σ_1	σ_2	$k = \sigma_1/\sigma_2$
1	2.68	0.20	13.65	2.49	-0.05	-54.23	2.59	0.09	27.62
2	2.72	0.16	17.08	2.52	0.02	123.68	2.60	0.09	29.16
3	2.79	0.23	12.33	2.54	0.02	162.30	2.65	0.12	22.92
4	2.60	0.14	18.52	2.49	-0.03	-94.62	2.55	0.07	36.06
1-2-3-4	2.70	0.18	14.97	2.51	-0.01	-302.15	2.60	0.09	28.26
Reference	3.10	0.00	∞						

Table 5b: Determination of Hole Surface Stresses Perpendicular to the x- and y-axes using Data from Individual and Combined Quadrants for the Plate with an Elliptical Hole ($a/b = 2$); Far Field Stresses: $\sigma_1 = 3.1$, $\sigma_2 = 0$

	Dark Field Isochromatics			Light Field Isochromatics			Combined Dark and Light Field Isochromatics		
Quadrant	σ_A	σ_B	$k_{AB} = \sigma_A/\sigma_B$	σ_A	σ_B	$k_{AB} = \sigma_A/\sigma_B$	σ_A	σ_B	$k_{AB} = \sigma_A/\sigma_B$
1	2.55	14.02	0.18	2.85	13.28	0.21	2.67	13.66	0.20
2	2.67	14.27	0.19	2.74	13.37	0.21	2.69	13.71	0.20
3	2.61	14.57	0.18	2.76	13.47	0.21	2.68	13.95	0.19
4	2.58	13.66	0.19	2.81	13.26	0.21	2.67	13.47	0.20
1-2-3-4	2.61	14.14	0.18	2.79	13.35	0.21	2.69	13.71	0.20
Reference	3.10	15.50	0.20						

6 DISCUSSION

An inverse problem methodology is implemented to critically examine the problem of a homogeneous, isotropic biaxially loaded plate with a centrally placed elliptical hole. This methodology requires that the problem be examined initially with an analytical approach, and also with a finite element model, to decide which model reproduces the experimental results by Durelli and Murray[6] best, as either an infinite or finite plate. The results clearly show that the plate used in the experiments corresponds to a finite plate geometry and needs to be examined from that perspective. To gain some appreciation for the nonlinear least squares approach, which is used to implement the inverse problem methodology, it is found that it is fairly robust when varying levels of noise are taken into account in evaluating the far field stresses using an analytical model. The implementation of the inverse problem methodology using a finite element based approach is performed for three experimental sets of results for values of nominal far field stress ratio $k = 0$, 1, and ∞. Harvesting of data from all four quadrants, but using only a single quadrant finite element model, it is possible to reconstruct and represent the data obtained by this inverse problem methodology using composite images. These images clearly reflect the asymmetry that exists in the experimental data, and serves to

shed further light on the experimental procedures used: (a) the implementation of biaxial testing is difficult, even when performed by the best practitioners; (b) application of the vertical load seems to be more experimentally feasible than application of horizontal loading; and, (c) having flexibility in analytical or numerical modeling serves to shed light on the experimentation that is performed.

7 SUMMARY AND CONCLUSIONS

Several objectives have been accomplished by using an inverse problem methodology in this paper: (1) posing an inverse problem for a homogeneous, isotropic finite plate with a central elliptical hole in photoelasticity, i.e., consideration of this approach as a means to assess the far field stresses applied on the plate; (2) assessing the plate size needed to consider the existence of an elliptical hole with semi-axes ratio $a/b = 2$ as being in an infinite plate; (3) re-examining experimental results for a finite biaxially loaded plate with a central elliptical hole using finite elements to model the plate; and, (4) reconstruction of the experimental results which allows a careful assessment of the limits of the experimental and theoretical models.

In summary, application of experimental or analytical and/or numerical work alone does not allow to fully understand a practical problem. It seems that the better approach is to use experimentation as a means to collect full field experimental data, which is then used to perform the theoretical/numerical reconstruction of the experimental results. This allows a check on the actual experimental conditions that were to be addressed, e.g., applied far field stresses. At the same time this serves to reassess the theoretical/numerical model to determine what the correspondence is between the experiment and its theoretical framework. This opens up a new, more organized and methodical way to complement the use of experimental and analytical / numerical capabilities using an inverse problem methodology. This type of approach also serves to promote the posing and searching for the inverse problems inherent in solving direct problems, which helps in further clarifying the problem that is being addressed, with the potential of allowing the calculation of parameters which prior consideration did not permit.

8 REFERENCES

[1] G. Kirsch, Die theorie d. elastizitat u. d. bedurinisse d. festigkeitslehre. V. D. I., **42**(29), 799, (1998).

[2] C. E. Inglis, “Stresses in a Plate Due to the Presence of Cracks and Sharp Corners”, *Transactions of the Institute of Naval Architects*, **55**, 219-230 (1913).

[3] G. N. Savin, *Stress Concentration Around Holes*, ed. W. Johnson, New York, Pergamon Press, (1961).

[4] H. Neuber, *Theory of Notch Stresses: Principle for Exact Calculation of Strength with References to Structural Form and Material, 2nd Edition*, Springer Publishers, Berlin, (1958).

[5] A. J. Durelli and W.M. Murray, “Stress distribution around a circular discontinuity in any

two dimensional system of combined stress", *Proceedings of the 14th Semi-Annual Eastern Photoelasticity Conference*, Yale University, New Haven, CT, (1941).
[6] A. J. Durelli and W. M. Murray, "Stress distribution around an elliptical discontinuity in any two-dimensional, uniform and axial system of combined stress", *Proceedings of the Society for Experimental Stress Analysis*, **1**(1), 19-31, (1943).
[7] E. G. Coker and L. N. G. Filon, *A treatise on photo-elasticity*, Cambridge University Press, Cambridge, England, (1957).
[8] M. M. Frocht, *Photoelasticity, Vol. II.*, John Wiley & Sons, Inc., New York, (1948).
[9] A. Nadai, R. Baud, and A. Wahl, "Stress Distribution and Plastic Flow in an Elastic Plate With a Circular Hole", *Mechanical Engineering*, **52**(3), 187-192, (1930).
[10] A. J. Durelli, V. J. Parks, and H. C. Feng, "Stresses Around an Elliptical Hole in a Finite Plate Subjected to Axial Loading", *Transactions of the ASME: Journal of Applied Mechanics, Series E*, **88**(1), 192-195, (1966).
[11] M. Isida, "On the Tension of a Strip with a Central Elliptic Hole", *Transactions of the Japan Society of Mechanical Engineers*, **21,** 514, (1955).
[12] N. A. Rubayi and A. D. Nana, "Photoelastic Stress Analysis of an Elliptical Hole in a Thick Plate Subjected to Uniform In-Plane Compressive Loading", *Experimental Mechanics*, **25**, 105-114, (1985).
[13] V. Tesar, "La photoelasticimetric et ses applications dans les constructions aeronautiques", *La Science Aerienne*, Sept-Oct, 372, (1932).
[14] A. J. Durelli, and K. Rajaiah, "Determination of Strains in Photoelastic Coatings", *Experimental Mechanics*, **20**(2), 57-64, (1980).
[15] J. F. Cardenas-Garcia, J. Hashemi, and A. J. Durelli, "The practical use of the hole method in photoelasticity", *Mechanics Research Communications*, **22**(3), 239-244, (1995).
[16] J. F. Cardenas-Garcia, Y. L. Tian, J. Hashemi, and A. J. Durelli, "A Least-Squares Approach to the Practical Use of the Hole Method in Photoelasticity", *Journal of applied mechanics*, **64**(3), 576, (1997).
[17] J. F. Cardenas-Garcia, "Catalogue of photoelastic fringes for a biaxially loaded infinite plate with a hole", *Strain*, **35**(3), 97-104, (1999).
[18] J. F. Cardenas-Garcia, "Photoelastic inverse problem solution for a biaxially loaded infinite plate with a hole", *Strain*, **35**(4), 131-138, (1999).
[19] J. F. Cardenas-Garcia, "The hole drilling method in photoelasticity - application of an optimization approach", *Strain*, **36**(1), 9-17, (2000).
[20] A. J. Durelli and W. F. Riley, *Introduction to photomechanics*, Prentice-Hall Book Co., Inc., Englewood Cliffs, NJ, (1965).
[21] J. W. Dally and W. F. Riley, *Experimental Stress Analysis, 3rd ed.*, McGraw-Hill, New York, (1991).
[22] A. E. Green and W. Zerna, *Theoretical Elasticity*, Oxford University Press, Glasgow, Great Britain, 322-372, (1969).
[23] S. G. Lekhnitskii, *Anisotropic Plates, translated by S. W. Tsai and T. Cheron*, Gordon and Breach Science Publishers, New York, NY, 57-217, (1968).

[24] R. J. Sanford, "Determining Fracture Parameters with Full-Field Optical Methods", *Experimental Mechanics*, **29**, 241-247, (1989).
[25] R. J. Sanford and J. W. Dally, "A General Method for Determining Mixed Mode Stress Intensity Factors from Isochromatic Fringe Patterns", *Engineering Fracture Mechanics*, **11**, 621-633, (1979).
[26] R. J. Sanford, "Application of the Least-squares Method to Photoelastic Analysis", *Experimental Mechanics*, **20**(6), 192-197, (1980).
[27] M. Abramowitz and I. A. Stegun, eds., *Handbook of Mathematical Functions with Formulas, Graphs, and Mathematical Tables, 9th printing*, Dover, NY, 18, (1972).
[28] K. Levenberg, "A method for the solution of certain nonlinear problems in least squares", *Quarterly of Applied Mathematics*, **2**, 164-168, (1944).
[29] D. W. Marquardt, "An algorithm for least squares estimation of nonlinear parameters", *Journal of the Society for Industrial and Applied Mathematics*, **11**, 431-441, (1963).